Deterministic risk assessment of hydrogen leak from a fuel cell truck in a real-scale hydrogen refueling station

Fangnian Wang [a], *Jianjun Xiao* [a,*], *Mike Kuznetsov* [a], *Wolfgang Breitung* [a], *Binbin He* [a], *Shengchao Rui* [a], *Shangyong Zhou* [a], *Thomas Jordan* [a], *Ke Song* [b,c], *Lijun Zhang* [b,c]

[a] *Institute for Thermal Energy Technology and Safety, Karlsruhe Institute of Technology, Hermann-von-Helmholtz-Platz 1, 76344 Eggenstein-Leopoldshafen, Germany*
[b] *School of Automotive Studies, Tongji University, Shanghai 201804, China*
[c] *National Fuel Cell Vehicle and Powertrain System Engineering Research Center, Tongji University, Shanghai 201804, China*

ARTICLE INFO

Keywords:
Deterministic risk assessment
Hydrogen safety
Deflagration
Hydrogen refueling station
CFD
GASFLOW-MPI

ABSTRACT

Deterministic risk assessment for hydrogen installations offers an integrated solution for H_2 risk assessment, incorporating a hydrogen release model, a site-specific 3D geometry model, a Computational Fluid Dynamics (CFD) tool, and a consequence analysis methodology. Empirical engineering models expedite the preparation of source terms and harm evaluations, while CFD generates 3D contours of radiation and overpressure loads. A case study is provided by investigating a gaseous hydrogen leak of a truck in a refueling station with a large roof. The effects of leak diameters, roof configurations, and ignition locations on hydrogen dispersion, combustion, and hazard analysis are examined. Results indicate that the majority of the burnable cloud accumulates in a half-meter layer under the ceiling, diminishing within a minute. The impact of thermal radiation on individuals is insignificant, but overpressures increase the likelihood of structure failures, indirectly affecting human fatality. These findings inform the optimization of refueling station design and safety management.

* *Corresponding author.*
E-mail address: jianjun.xiao@kit.edu (J. Xiao).

1. Introduction

Hydrogen is emerging as a crucial energy carrier that provides environmentally friendly energy to end-users [1]. However, the widespread acceptance and use of hydrogen in society necessitate significant advancements in the field of hydrogen safety. This discipline of science and engineering is concerned with the safe production, handling, and utilization of hydrogen in various industries and society [2]. Hydrogen exhibits unique properties that distinguish it from conventional hydrocarbon fuels. These properties include the ability to cause embrittlement in metals, a low boiling point and density, a low ignition energy, a wide flammability range, a high laminar burning velocity, and a tendency to undergo deflagration-to-detonation-transition (DDT) under specific conditions [3]. Consequently, flash/jet fires and explosions pose significant hazards for hydrogen installations, necessitating specific measures for reducing the risk to an acceptable level. Prevention and mitigation are required not only for relatively simple systems such as fuel cells, vehicles, and refueling stations but also for complex industrial facilities like the nuclear power plants' containment systems [3]. The recurrence of low-probability severe-consequence accidents [4,5] indicates that the common feature is a limited understanding of the actual hydrogen hazard before the accidents.

H_2 risk assessment aims to systemize knowledge and uncertainties concerning phenomena and processes, provide a foundation for evaluating what is tolerable and acceptable regarding the potential risks, and optimize different design options and risk-reducing measures to minimize the potential risks [6]. Quantitative Risk Assessment (QRA) is a beneficial tool for identifying deficiencies and enhancing safety performance in complex hydrogen systems [6], such as the HyRAM toolkit from SANDIA [7]. The schematic of QRA is outlined in Fig. 1 left side. It is worth noting that the term 'QRA' may refer to either 'quantitative risk analysis' or 'quantitative risk assessment,' which encompasses both risk analysis and the evaluation of the analysis results [8]. QRA assists in decision-making by assessing whether the risk of failure in a system is As Low As Reasonably Practical (ALARP). QRA involves identifying potential scenarios, estimating their consequences and frequencies, and analyzing the risks they pose to people, the environment, and assets. The consequences (number of the injured, deaths, or property damage) and the frequencies (number of occurrences per year) rely on industry standards, facts, historical/statistical databases, and other relevant sources.

However, the scenarios corresponding to worst cases (e.g., large-bore rupture of the hydrogen leak or ignition at specific times and locations) are not always emphasized in QRA. These scenarios can be identified through brainstorming exercises such as HAZOP and What-if analysis, or imposed by the authorities. They can be based on accidents that have occurred in the past, such as the hydrogen explosion in the Fukushima nuclear disaster [5]. As a result, it is crucial to evaluate the risks associated with worst-scenarios. This led to the development of the Deterministic Risk Assessment (DRA) concept, which emerged from a team in an organization that develops complex software systems, including CFD codes, such as FLACS, GASFLOW-MPI, ANSYS/CFX/FLUENT, STAR-CCM+, OpenFOAM, etc. [9–11].

CFD codes utilize a detailed Computer-Aided Design (CAD) model to generate CFD meshes, perform the hydrogen dispersion, combustion, explosion simulations, and 3D visualization automatically based on the time-dependent stepwise of a leak from pipe/tank and immediate/delayed ignition within the flammable volume. In worst-scenarios, which cause severe thermal and pressure loads, it may need to optimize risk-reducing measures by identifying the hydrogen detector layout and risk mitigations, etc. Practically, it is required to complete the relevant simulations fast in the iterations if the risk evaluation is unacceptable. Therefore, the DRA framework is not limited to the CFD tool, but is also comprised of various utility programs and libraries integrated into the framework. These include a worst-scenarios generator (PSA and QRA support), source term models for leaks, a pre-/post-process, libraries of consequence models, frequency models, harm criteria of fire and overpressure, etc. As a result, DRA complements the traditional risk assessment QRA considerably by providing interactive 3D information for safety design, safety training, emergency mitigation, and other aspects of risk management within organizations [8].

The main limitation of the DRA concept is that the complete implementation requires a dedicated user who refers to a person or a team responsible for creating and maintaining the 3D model of the installation, as well as conducting risk assessments and simulations using the models [8]. The user requires specialized knowledge and training in 3D modeling, risk assessment, and simulation tools, which may not be feasible for all users. Human errors could be a significant challenge in risk assessment, as they may introduce biases that could impact the risk analysis process. On the other hand, conducting CFD simulations for hundreds of cases can be a time-consuming process when investigating statistical results, such as the occurrence frequency of a certain overpressure. The use of artificial intelligence [12] or proper orthogonal decomposition [13] may provide a solution to this challenge. Recent advances in machine learning have shown a promising ability to forecast solutions for partial differential equations. Specifically, trained neural networks have been shown to make accurate approximations in a fraction of the time compared to traditional CFD simulations [12].

Hydrogen fuel cell technology is a promising alternative for heavy-duty trucks, offering a similar driving range and refueling time to gasoline-powered trucks [14]. In addition, the predictable travel routes of the trucks reduce the barriers to the development of hydrogen refueling infrastructures, facilitating the widespread adoption of hydrogen fuel cell technology. Hydrogen safety is highly dependent on the configuration of the installations. Currently, hydrogen refueling stations are often integrated with petrol stations and utilize the same roof structure to save infrastructure investment, increase inventory, and accelerate the development of hydrogen energy. It makes the refueling station less safe because such big roofs promote possible hydrogen gathering and then flame acceleration. In the contrary, in the presence of hydrogen the roof should have regular gaps or chimneys to avoid hydrogen accumulations in dangerous concentrations. Extensive research has been conducted by scholars to assess

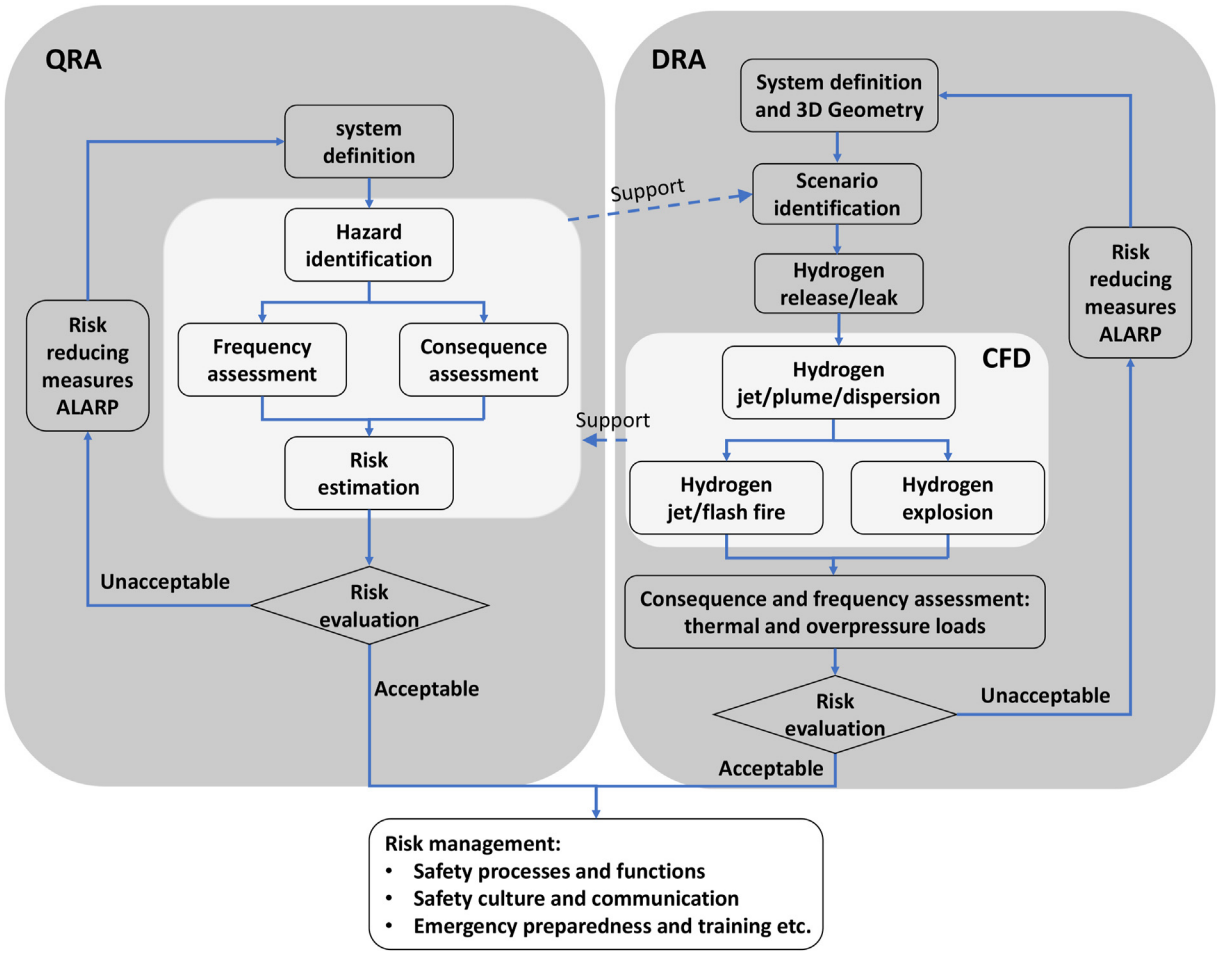

Fig. 1 – Approaches of quantitative and deterministic hydrogen risk assessment.

the safety of hydrogen in various scenarios, particularly with regard to fuel cell vehicles [11,15]. However, few investigations of the potential risks associated with larger amounts of hydrogen leak from trucks compared to normal cars in a refueling station with a large covered roof, represent significant knowledge gaps that require attention.

This paper aims to systemize and consolidate the DRA concept of hydrogen safety assessment and apply it to a hydrogen leak from a fuel cell truck in a real semi-confined refueling station with a large roof using CFD tool GASFLOW-MPI and empirical engineering models. This step-by-step detailed case study verifies the effectiveness and feasibility of the DRA method for assessing the risk of a typical hydrogen installation.

2. Deterministic risk assessment

DRA represents a comprehensive and integrated approach to assessing the H_2 (or other flammable gases) risks in complex systems. The following discussion provides key features of the DRA framework and illustrates how it can be implemented to analyze H_2 risk and enhance the risk management capacity by users.

2.1. *Approach description*

The primary motivation behind the implementation of DRA is to prevent and mitigate significant losses in the hydrogen industry and society. This is achieved through the integration of cutting-edge modeling tools (CFD and fast-running engineering models) in a unified framework for H_2 risk assessment and management, such as improving risk awareness and safety culture. The typical steps required to conduct a DRA are outlined in Fig. 1 right side. The implementation of DRA in a complex industrial plant involves the use of a highly detailed, site-specific 3D geometry model. This model serves as a means for interactive communication among stakeholders and enables the utilization of advanced CFD tools for simulating and visualizing the consequences models.

The process of establishing a DRA for a specific H_2 installation typically involves several steps, such as:

1. Importing or constructing a comprehensive 3D geometry model (meshes generated based on the detailed geometry of hydrogen installation) that is capable of supporting CFD simulations.
2. Identifying and registering the worst-scenarios. This can be achieved through the use of the Probabilistic Safety

Assessment (PSA) method and brainstorming exercises that can help determine the most severe accidents with high probability. These worst-cases can also be proposed by the processes of hazard identification, frequency/consequence assessments, and risk evaluation within the QRA approach.

3. Classifying the hydrogen (or other burnable gas) release sources. According to the worst-scenarios and the system design, hydrogen release sources of the most likely accident scenarios, such as hydrogen release flow rate, local pressure, and temperature can be obtained by empirical integrated engineering models or CFD calculations.
4. Initializing the species and inventory of hazardous materials, heat transfer parameters, potential ignition sources present within the 3D geometry model, and representative ambience boundary conditions (e.g., wind, ventilation, fan, and other engineered systems if applicable). Simulating a representative set of hydrogen release jet/plume and dispersion in an installation, which provides the necessary gas distribution and flow field data for indicating the worst ignition moment according to the location, mass, and volume of the accumulated hydrogen, and for further simulating the hydrogen combustion or explosion.
5. Simulating a representative set of the scenarios of jet fire (immediate/delayed ignition of a continuous release), fireball (immediate ignition of an instantaneous release), fireball-jet fire (delayed ignition of a continuous release), flash fire (delayed ignition of a continuous/instantaneous release), and pool fire (liquid hydrogen) based on the release conditions, to evaluate and mitigate fire hazards.
6. Simulating a representative set of explosion scenarios (delayed ignition) based on the dispersion of a continuous/instantaneous release to assess and mitigate the risks of explosions (typically, the overpressure and thermal effect on humans and structures).
7. Calculating and visualizing thermal and pressure load contours within the 3D geometry model, estimating the effect (harm) on human and structure caused by physical parameters such as radiative or convective heat flux, and pressure loads.
8. Evaluating the risk via harm criteria, safety standards, and legislations, iterating the processes to determine the appropriate safety measures, ultimately providing a comprehensive overview of the risks associated with the facility and developing effective risk management strategies.

2.2. *Physical models*

- **CFD tool**

Accidents in installations involve various fluid flows with or without chemical reactions in complex geometries, including the release and dispersion of dangerous substances, fires, and explosions of burnable gas or dust. Such hazardous materials may consist of flammable, asphyxiating, toxic, radioactive materials, in gaseous, liquid, solid phases, or heterogeneous systems. The CFD tool GASFLOW-MPI developed at Karlsruhe Institute of Technology (KIT), efficiently solves the three-dimensional compressible Navier-Stokes equations with multi-components. GASFLOW-MPI is suitable for simulating complex flows with various species [10]. The ICE'd-ALE numerical solution algorithm, which is valid for flows at wide ranges of Mach numbers, was adopted in the code [16,17]. GASFLOW-MPI incorporates several turbulent flow models, including RANS-based models, Detached Eddy Simulation (DES), and Large Eddy Simulation (LES) [18,19]. Additionally, the code can simulate combustion using diverse models, such as reaction progress variable-based models and multiple-step chemical reaction models. The code has been used in the safety analysis of many large-scale engineering applications [5], and the calculations can run automatically on a server and/or in the cloud. The turbulence model, combustion model, and the thermal radiation model are summarized in the supplementary data.

The process of validation and documentation poses a significant challenge for CFD developers that aim to describe a broad range of physical phenomena, including different initial and boundary conditions. GASFLOW-MPI capabilities of simulating all-speed flows in one solver with a wide range of Mach number [10], turbulent flows [18,19], combustion [20,21–24], and conjugate heat transfer have been well-validated through extensive testing and analysis of experiments. GASFLOW-MPI imports a 3D model of the hydrogen facility to set up to simulate hydrogen release jet/plume and hydrogen dispersion under the accident sequences. The modeling evaluates the turbulence effects and the influence of wind and engineered systems, which ultimately determines the areas where hydrogen accumulation is likely to occur and where there is a high probability of an explosion. GASFLOW-MPI can predict flame propagation of hydrogen combustion ignited at various locations, and evaluate the potential risk to humans and structures. The flame may start initially as a slow quasi-laminar deflagration, and it will preferentially propagate in the direction of high burning rates, generally towards the richer hydrogen mixtures and into regions with high turbulence intensity. The flame can induce a transition from slow laminar to fast turbulent deflagration or even undergo a transition to detonation. It is essential to model these slow and fast deflagrations with an appropriate all-speed numerical model.

- **Hydrogen release model**

Hydrogen release is modeled as the isentropic flow through an orifice and expands it to atmospheric pressure. Three key parameters of interest in hydrogen release are the pressure, temperature, and mass flow rate, which can be calculated using the orifice and notional nozzle models with assumptions and the library of fluid properties (e.g. CoolProp) as the method used in HyRAM+ [25]. At the beginning of the release from a high-pressure tank, for instance, the flow is choked through the orifice. The blowdown phase is of great importance for the hydrogen release, since most of the hydrogen mass is already released in this period. The ambient pressure is much smaller than the pressure in storage [20], thus, the choked flow is the focus of hydrogen blowdown. The thermal conditions (T and P) at the orifice can be solved using an assumed isenthalpic expansion [25,26],

$$\begin{cases} s(T,P) = s_0 \\ \dfrac{(a(s_0,P))^2}{2} + h(s_0,P) = h_0 \end{cases}, \quad (1)$$

where $s(T, P)$ is the entropy at the orifice, equaling the upstream hydrogen entropy s_0. CoolProp is used to calculate the entropy (s_0) and enthalpy (h_0) of the fluid upstream of an orifice, using the initial specified pressure and temperature in the tank. CoolProp is then used to calculate the fluid enthalpy (h), temperature (T), and sonic velocity (a) of the choked flow at atmospheric pressure, with the same entropy as the upstream fluid (s_0). In the case of choked flow, the calculation is finished when the solution of the system of equations is satisfied, and the hydrogen flow at the orifice is at pressure P, temperature T, and has a velocity equal to the speed of sound (a). The orifice is assumed to be circular, characterized by its diameter (d), and a coefficient of discharge (C_d). When the velocity and density $\rho(T, P)$ of the hydrogen at the orifice are known, the mass flow rate can be calculated by $\dot{m} = C_d \frac{\pi}{4} d^2 \rho a$. The transient process of a storage tank emptying can be calculated based on the conservation of energy and mass, as demonstrated by Hosseini et al. [27].

- **Harm assessment model**

Engineering models of consequence and frequency assessments are also used in the DRA approach. The consequences of fire hazards may include harm to personnel, equipment, or facilities due to high gas temperatures, radiant heat fluxes, or direct exposure to hydrogen flames. Another significant hazard is the explosion of hydrogen released accidently, which may or may not happen instantaneously. The potential consequences of such explosions on people, structures, or equipment may involve blast wave overpressure effects, impact from fragments generated by the explosion, or building collapse. Harm criteria serve as a means to translate the results of accident consequences to a likelihood of harm to individuals, structures, or components. Harm criteria are established by the use of thermal and overpressure thresholds for indicating the consequence levels or continuous functions that link the hazard level to the probability of damage [28]. The thermal and mechanical loads on humans and structures resulting from the combustion process (slow deflagration, fast deflagration, or detonation) are evaluated from the 3D simulation by storing heat flux and overpressure histories spatially. The prevailing load categories are mainly determined by the ignition time and location. Thermal dose from standing diffusion flames can result in human burns. Exposures to flames or radiant heat fluxes from fires can cause first-, second-, or third-degree burns, as well as breathing difficulty and respiratory damage. Whereas, pressure waves, impulses, and possible impacts from combustion-generated missiles can lead to human fatalities and structural failure. It is, therefore, imperative to define hazard distances during incidents for emergency management.

Probit functions translate the thermal dose level and overpressure level ΔP_{max} to a probability of human injury, human fatality, and structure failure. A probit function is the inverse cumulative distribution function associated with the standard normal distribution. Probit functions are particularly useful in hydrogen safety assessment since they can provide harm probabilities for the range of accidents via the transformation between percentage p and probit Y,

$$Y \quad 5 = \sqrt{2}\,\mathrm{erf}^{-1}\,(2p\,/\,100 \quad 1). \quad (2)$$

The thermal dose probit functions for human response based on Eisenberg [29] study are,

$$Y_{1^{st}-degree\ burn} = \quad 39.83 + 3.0186 \ln\left(q^{4/3}t\right), \quad (3)$$

$$Y_{2^{nd}-degree\ burn} = \quad 43.14 + 3.0186 \ln\left(q^{4/3}t\right), \quad (4)$$

$$Y_{3^{rd}-degree\ burn} = \quad 38.48 + 2.56 \ln\left(q^{4/3}t\right), \quad (5)$$

where q is the radiant heat flux and t is the exposure time.

The probits of human fatality due to lung hemorrhage and structure failure with total damage provided by Eisenberg [29] are represented by,

$$Y_{\text{human fatality}} = \quad 77.1 + 6.91 \ln\left(\Delta P_{max}\right), \quad (6)$$

$$Y_{\text{structure failure}} = \quad 23.8 + 2.92 \ln\left(\Delta P_{max}\right). \quad (7)$$

3. Case study

3.1. Geometry model

As shown in Fig. 2, a simplified model of a large-scale hydrogen refueling station, located in Beijing, China [30], was utilized to investigate hydrogen release, dispersion, and combustion under hypothetical accident scenarios. The station is equipped with eight hydrogen dispensers and sixteen hoses in total, with a capacity to refuel up to 4.8 tons of hydrogen, approximately 600 vehicles per day. The increased likelihood of hydrogen leakage from the tanks and pipelines of hydrogen-powered vehicles is expected due to the high number of vehicles refueled in the station.

Fig. 2 depicts the 3D geometric model used for the GASFLOW-MPI simulations. The computational domain is 20 m, 28 m, and 6.6 m in the X, Y, and Z directions, respectively. The distance between the ground and the ceiling is 5 m, and the roof has a thickness of approximately 1.6 m (Z = 5.0 m–6.6 m). The centreline of the truck is situated at Y = 4.9 m. The truck's dimensions are 13 m (length), 2.45 m (width), and 3 m (height). The truck is equipped with eight hydrogen tanks, each with a volume of 170 L, and the pressure and temperature inside each tank are 35 MPa and 300 K, respectively. The eight tanks collectively provide a storage capacity of around 32 kg of fuel. However, the leak from one tank with a hydrogen inventory of about 4 kg hydrogen is assumed in current research. A leak, if it occurs at the center of the refueling station, could be one of the worst scenarios. However, considering the convenience for refueling and aligning with the actual situation, the leak is placed in the center of the station as far as possible, as shown in Fig. 2. There are fifty monitor points in total, including P1–P25 which are 5 cm below the ceiling, and P26–P50 which are 5 cm above the ground. The computational mesh was automatically generated based on the geometric model shown in Fig. 2. A

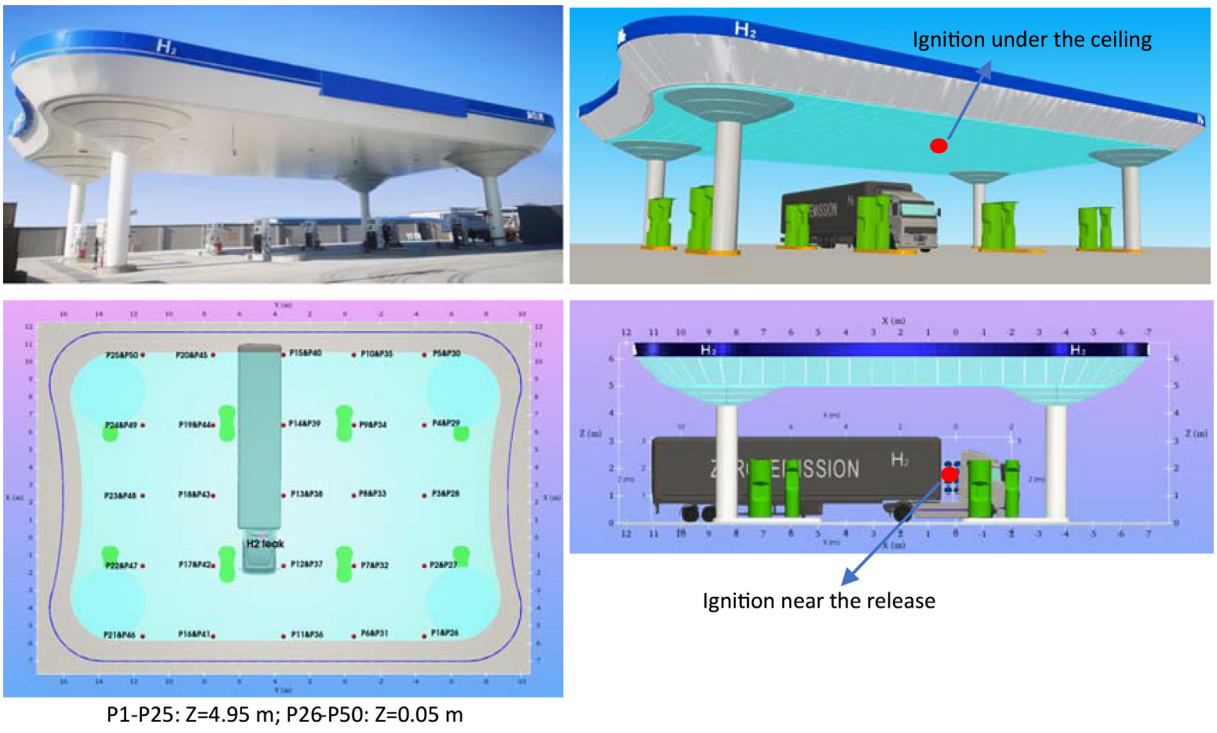

Fig. 2 – Geometric model for 3D GASFLOW-MPI simulations.

sensitivity analysis was conducted, and the mesh system with 2,268,000 cells (135 cells on X-axis, 168 cells on Y-axis, and 100 cells on Z-axis) was found to be suitable for our investigation. The mesh is refined in areas where hydrogen release, accumulation, and combustion occur, as shown in the following mesh figure. Specifically, we focused on three specific locations: under the ceiling, above the ground, and in the hydrogen release jet zone. These areas were subjected to mesh refinement, as the phenomena occurring in them are of particular interest in the context of hydrogen safety in the current cases. In order to minimize pressure wave reflection at the open boundaries, additional cells were stretched until each constant pressure boundary. In order to minimize pressure wave reflection at the open boundaries, additional stretched cells were added to each constant pressure boundary. The truck and structure of the refueling station are set as solid obstacles in the CFD modelling.

3.2. *Hydrogen release*

Hydrogen gas can leak through the crack orifice in the hydrogen tank, which is located between the container and the trailer. The leaked hydrogen forms a horizontal impinging jet that attaches to walls or structures, causing the hydrogen sonic jet to transform into a plume with a relatively lower velocity. It is conservative from a safety perspective, since slower hydrogen dispersion could lead to a higher accumulation of hydrogen. In our calculation cases (Table 1), the hydrogen gas discharges horizontally and hits the back wall of the container. Two tests were also conducted to study hydrogen combustion during high-risk moments of the explosions but with different ignition locations, as seen in Fig. 2. The exact coordinates of these two locations are (0.12 m, 4.9 m, 1.3 m) of the ignition near the release and (0.45 m, 1.5 m, 4.9 m) of the ignition under the ceiling. One of the calculations did not include a refueling station ceiling to examine the influence of the ceiling on hydrogen distribution. The effect of the wind was not considered currently.

The coordinates of the hydrogen leak location is (0 m, 4.9 m, 1.2 m), as seen in Fig. 2. The discharge coefficient c_d varies considerably with changes in area ratio and the Reynolds number. A discharge coefficient $c_d = 0.6$ may be taken as standard, but the value varies noticeably at low values of the Reynolds number. So, the discharge coefficient

Table 1 – GASFLOW-MPI calculation cases.

Cases	Diameter (mm)	Ceiling	Combustion	Ignition time (s)	Ignition location
1	10	yes	no	/	/
2	5	yes	no	/	/
2-com-1	5	yes	yes	15	near the leak
2-com-2	5	yes	yes	15	ceiling
3	2	yes	no	/	/
4	0.5	yes	no	/	/
5	5	no	no	/	/

for the choked flow in our cases is set 0.6. The initial pressure in the hydrogen storage tank is 35 MPa, the temperature is 300 K, and the total mass of one tank is 4 kg. Following the engineering model of hydrogen release, the cases of 1, 2, 3, and 4 with various orifice diameters are calculated, as shown in Fig. 3. The parameters of pressure, temperature, and mass flow rate are considered as source terms in the GASFLOW-MPI simulation models. The trend of the hydrogen release parameters is decreasing exponentially, however, the release speed with a smaller orifice diameter is faster. The release through a 10 mm orifice is completed in 30 s, while the release through a 5 mm orifice takes 100 s. When the release time is sufficiently long and the pressure is balanced, the mass flow rate will tend to approach zero. In our analysis, we focused on ensuring that the release time was adequate to identify the worst situation of interest.

3.3. *Hydrogen dispersion*

Hydrogen dispersion in the refueling station is highly impacted by various hydrogen leak diameters (10 mm, 5 mm, 2 mm, and 0.5 mm). Fig. 4 presents the total mass and volume of the burnable hydrogen-air clouds (4–75% of hydrogen volume). The mass and volume of burnable hydrogen-air clouds reach their peaks in 7–30 s, depending on the orifice diameters. The larger the orifice diameter, the higher peaks of the mass and volume, but the faster their decrease. The mass flow rates of the leak, as shown in Fig. 3, mainly determine these processes. Comparing the dashed and solid curves of total H_2 mass and volume in Fig. 4, it is found that 90% of the hydrogen accumulates in the zone under the ceiling half-meter, very close to a 60 cm layer under the ceiling in a road tunnel [31]. The average hydrogen concentration is over 10%, even over 35% in Case 1 and 2, as seen in Fig. 4. We can conclude that the 15-s delay after a leak accident is a highly dangerous moment that may cause a hydrogen explosion under the ceiling. Therefore, emergency management should be implemented immediately in case of hydrogen leak accidents, and ignition sources close to the ceiling should be avoided as much as possible.

The hydrogen release is near completion after 50–150 s in Case 1, 2, and 3. As a result, the mass and volume of hydrogen are approaching less than 0.1 kg and 20 m^3, respectively, which is also observed in Case 4 with a small orifice size of 0.5 mm and in Case 5 without a ceiling. In Case 3, the mass decreased moderately and lasted relatively longer due to the small size of the orifice. In Case 4, the hydrogen dispersed and diluted quickly due to the small mass release rate of 2–3 g/s. In Case 1 and 5, the mass reduced to less than 0.1 kg in 50 s and approached zero in 100 s. These observations suggest that the

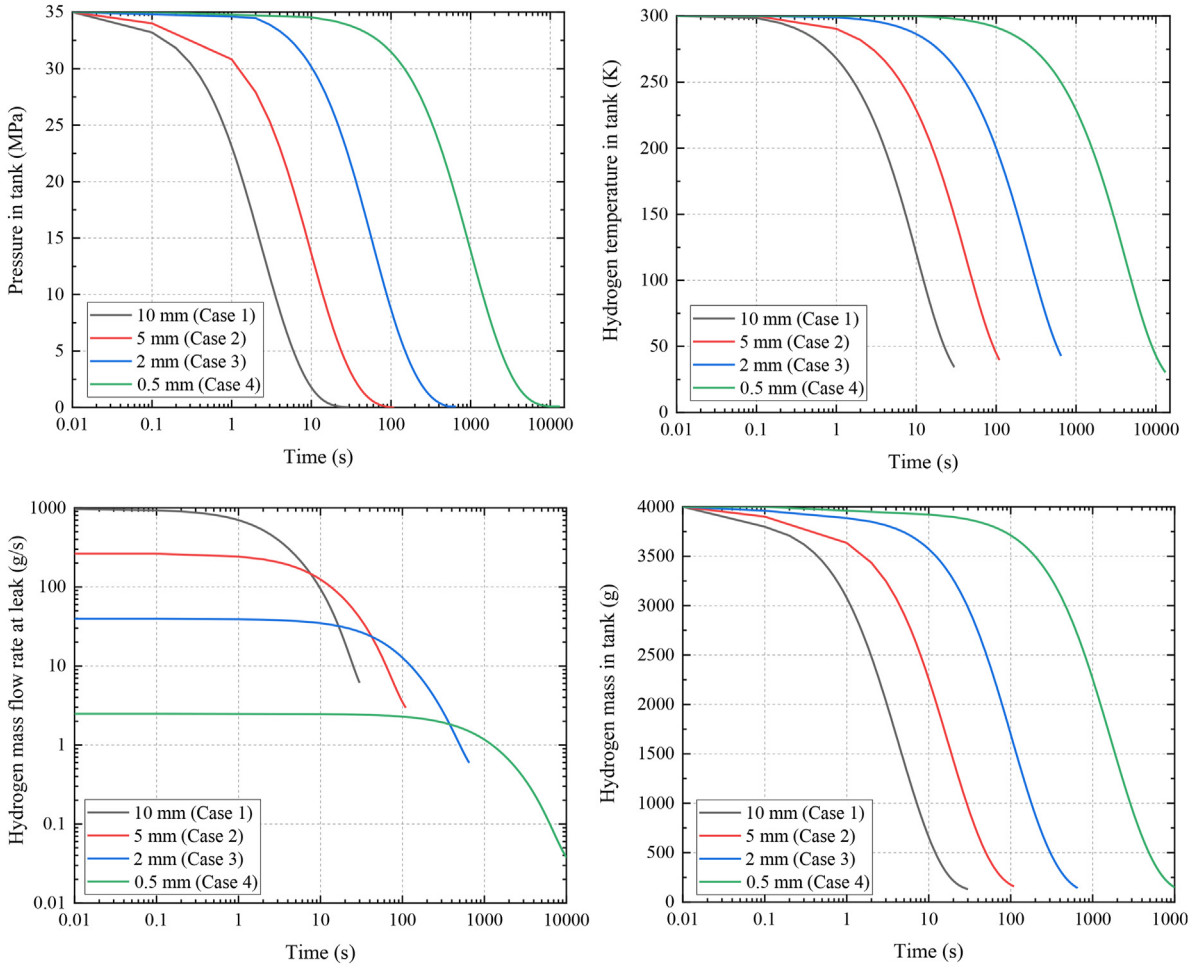

Fig. 3 – Pre-calculated parameters inside the hydrogen tank during blowdown.

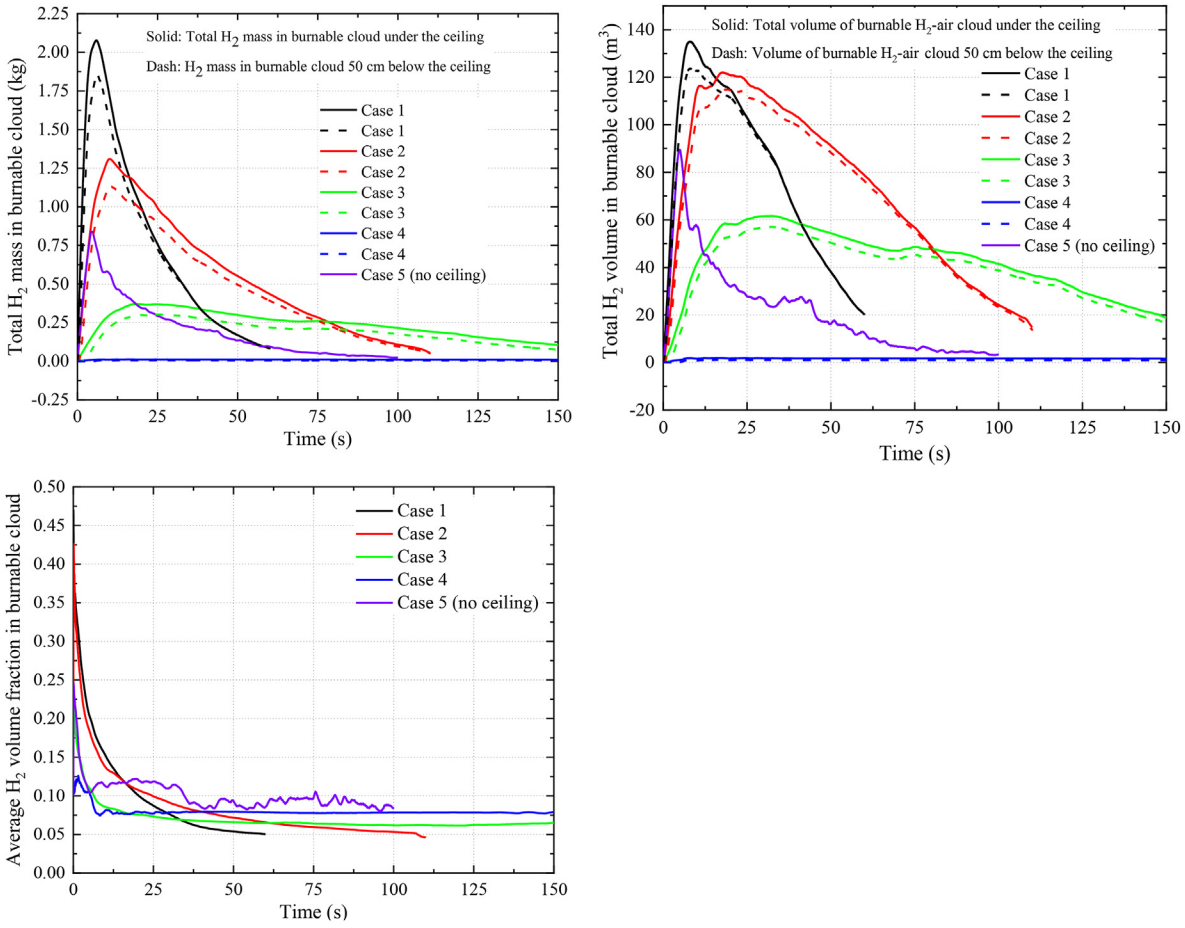

Fig. 4 – Total H_2 mass, volume, and average H_2 volume fraction in burnable cloud.

possibility of a hydrogen explosion in Case 3, 4, and 5 is much smaller than in Case 1 and 2. From all the comparison results, it appears that there is no hydrogen hazard after the leak accident after 3 min delay, regardless of the orifice diameter and the existence of a ceiling. Case 5 demonstrates the efficiency of smaller/no roof area, the higher its position, and the existence of a regular chimney on the roof to avoid hydrogen accumulation within burnable concentrations. We are planning to investigate the effects of roof coverage, type, and inclination in our future work. However, we can tentatively conclude that less roof coverage may be beneficial for H_2 safety.

The development of the hydrogen volume fraction and burnable hydrogen cloud in Fig. 5 provides further evidence of the hydrogen distribution at the 15-s mark. The hydrogen concentration before this time is higher, but the mass and volume are lower. After 15 s, the hydrogen disperses further, and the volume of the flammable gas mixture decreases due to the decreasing release. By 105 s after the release, the hydrogen concentration and burnable volume are significantly lower than they were at around 15 s. The volume evolution image is consistent with the results in Fig. 4. Based on the maximum mass and volume of flammable gas present at the station, and the persistence of relatively strong turbulence at the 15-s mark, it can be inferred that a potential ignition occurring at this point represents a large combustion zone and high overpressure, which could be one of the representative worst-scenarios for analyzing hydrogen risk.

3.4. *Hydrogen combustion*

Based on the hydrogen dispersion analysis, the most hazardous period after the release occurs approximately 15 s later, owing to the significant hydrogen mass of approximately 1.3 kg and a volume of around 120 m^3, which is stored under the ceiling. Compared to Case 1, which has an orifice diameter of 10 mm, Case 2 with a medium orifice diameter of 5 mm is more likely to experience a leak. A 5 mm orifice diameter is commonly assumed for the leak of buses, trains, and refueling stations that have larger hydrogen storage tanks like trucks [32]. In addition, as presented in Fig. 4, the hydrogen dispersion in the station reveals that the leak with a 5 mm orifice diameter has resulted in a large accumulation of hydrogen mass/volume under the ceiling. To assess the effect of ignition location, the combustion analysis of Case 2 was divided into two subcases (Case-com-1 and -2) with the ignition location near the leak and on the ceiling, respectively (see Table 1).

The blast wave propagation of Case-com-1 is depicted in Fig. 6. The time in the images is the relative time, meaning that hydrogen release has passed 15 s before the ignition. The blast wave originates from the ignition location near the tank

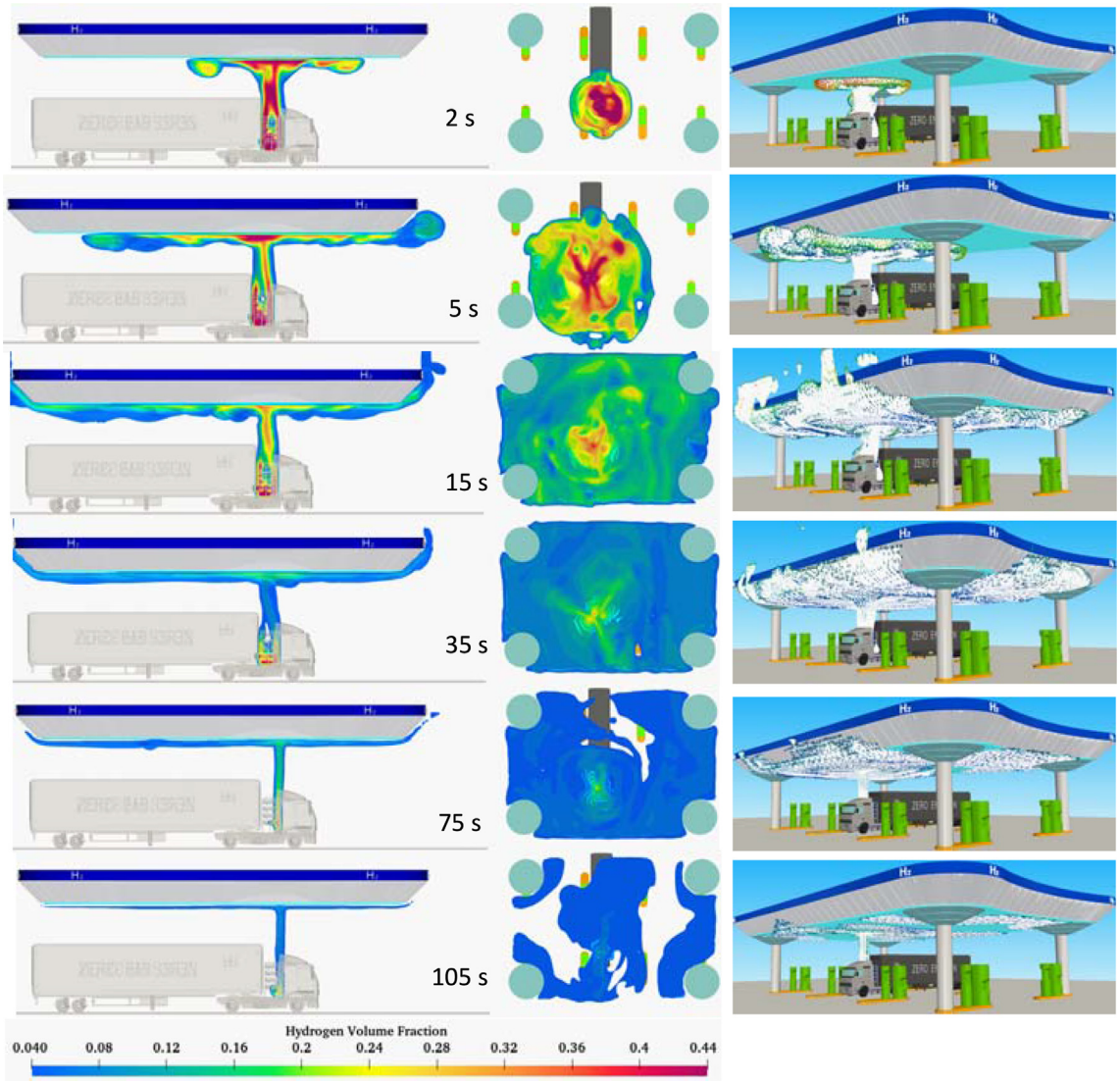

Fig. 5 – Hydrogen volume fraction and burnable hydrogen cloud (Case 2). Vertical cut: Y = 4.9 m, horizontal cut: Z = 4.95 m

and has a pressure of over 1.5 bar. It then propagates upwards to the ceiling and downwards to the ground within 13 ms. The ceiling and ground obstruct the wave, resulting in wave reflections, as seen in the image at 16 and 20 ms. The impact of the supporting cylinder on wave reflections can also be seen in the horizontal cut at 25 ms. The wave gradually weakens over time and space and occupies the entire station within 30 ms before propagating outside.

Fig. 7 presents the overpressure distribution of Case-com-1 and Case-com-2 below the ceiling and on the ground. The results indicate that the highest overpressures are located in the region above the hydrogen release. At locations 12, 13, and 18, the peaks of overpressure exceeding 70 and 40 kPa are observed at approximately 15 ms, respectively. In contrast, the maximum overpressures in other areas below the ceiling are less than 20 kPa. The peak overpressure presented here represents the maximum overpressure rise caused by the explosion. The peak overpressure observed at 30 ms in the top right image could be attributed to either a reflection or some numerical oscillation. The duration of this peak overpressure is extremely short, lasting only 0.01 ms, or even less. From the perspective of explosion consequences, the impulse should be significantly smaller when compared to the impulse around 15 ms. Consequently, we believe that the peak overpressure caused by the explosion is more important for subsequent hazard analysis than the momentary jump with such a negligible duration.

The overpressures decrease over time, which is consistent with the trend shown in Fig. 6. The overpressures on the ground also decrease oscillating over time, even reaching negative values. The overpressures below the ceiling are generally greater than that on the ground. Locations 37, 38, and 43 exhibit the highest overpressure, exceeding 20 kPa, precisely below the release zone. Therefore, it can be concluded that the area within 2–3 m of the hydrogen release is very hazardous.

In Case-com-2, the maximum overpressures near the hydrogen release point are approximately 20 kPa, which is much lower than the results obtained in Case-com-1. The presence of two distinct peaks and a time delay can be

Please cite this article as: Wang F et al., Deterministic risk assessment of hydrogen leak from a fuel cell truck in a real-scale hydrogen refueling station, International Journal of Hydrogen Energy, https://doi.org/10.1016/j.ijhydene.2023.09.114

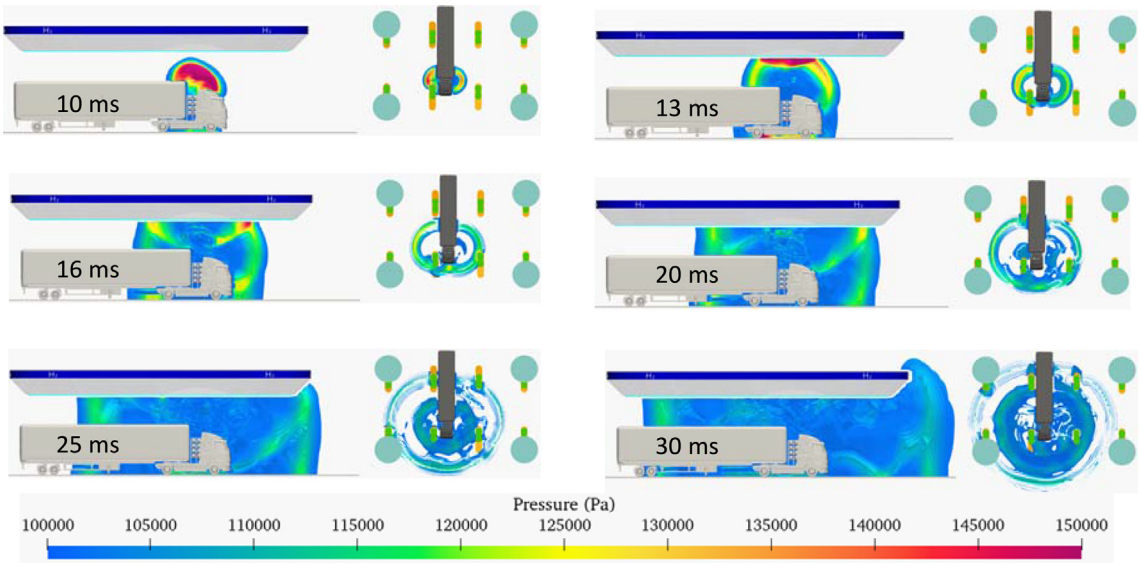

Fig. 6 – Blast wave propagation (Case-2-com-1). Vertical cut: Y = 4.9 m, horizontal cut: Z = 1.0 m

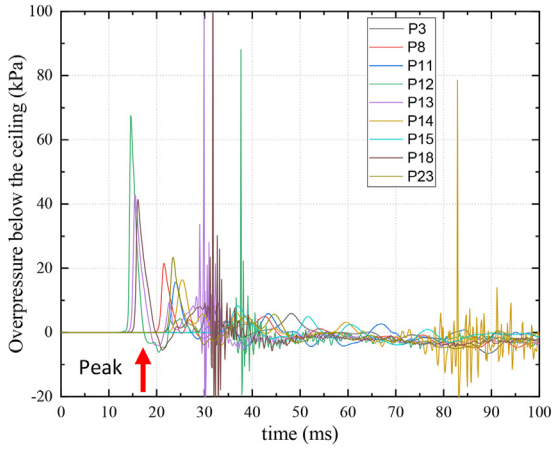

Case-2-com-1 overpressure ceiling

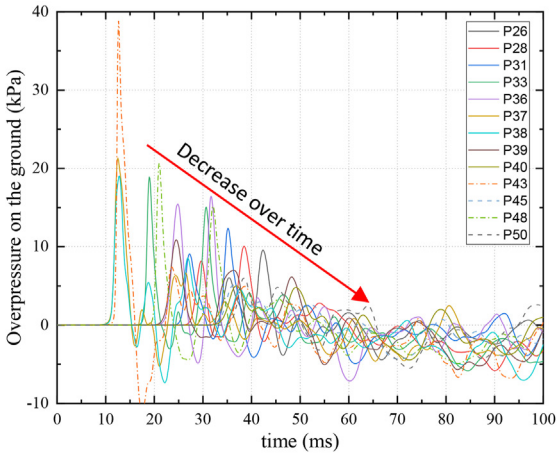

Case-2-com-1 overpressure ground

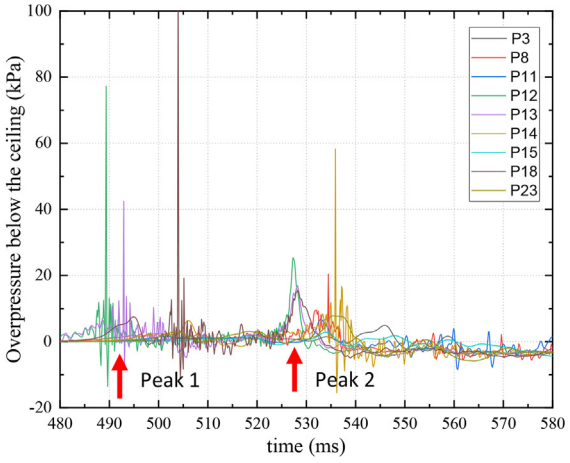

Case-2-com-2 overpressure ceiling

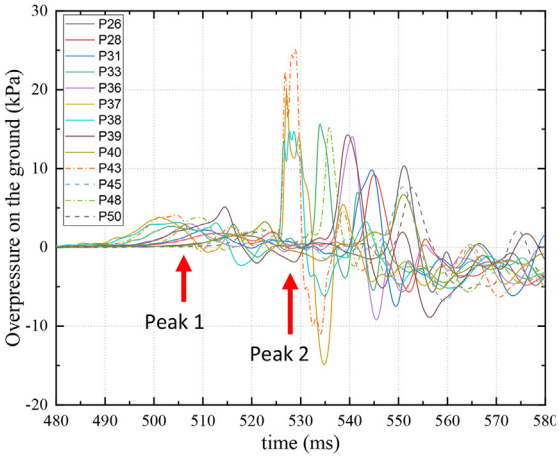

Case-2-com-2 overpressure ground

Fig. 7 – Overpressure close to ground and ceiling in Case 2.

attributed to continuous hydrogen deflagration first occurring under the ceiling and then in the release zone. As the flame propagates to the hydrogen release zone, the overpressure rapidly increases again, reaching peak pressure and subsequently fluctuating. The deflagration in the release zone generates higher overpressure during the period between 520 and 530 ms. Initially, overpressure on the ground increases moderately because the first hydrogen deflagration is far from the ground, and the wave generated on the ceiling propagates to the ground. The overpressure under the ceiling at 525 ms is lower than that on the ground because the distance from the ground to the core of the deflagration in the release zone is shorter than the distance from the ceiling. The maximum overpressure on the ground is slightly lower than in Case-com-1, with a difference of approximately 5 kPa, which can be attributed to the higher turbulence and a higher local hydrogen concentration in the vicinity of the ignition position in Case-com-1 resulting in a faster hydrogen deflagration speed, as seen the description of the turbulent flame speed S_T model in the supplementary data.

Fig. 8 depicts the temperature profile of combustion products in vertical and horizontal cuts, demonstrating the propagation of flame in Case-2-com-1 and Case-2-com-2 in the direction of flow and opposite to the flow direction, respectively. In Case-2-com-1, the flame originating from the release area propagates upward and eventually spreads over the entire region beneath the ceiling. Conversely, in Case-2-com-2, the flame originates from a corner below the ceiling and moves towards the release zone, in opposition to the gas flow. This implies that the flame propagation direction can be counter to the flow direction. As the downward-propagating flame should overcome the buoyancy of the combustion product, the speed could be smaller than the one of the upward flames [33]. This is one of the reasons that the maximum overpressure is lower in Case-com-2 than the one in Case-com-1. Nevertheless, in both cases, the flame intensity is higher in the release zone, as the turbulence is more prominent in this region. The flame remains confined to the hydrogen accumulation area below the ceiling and never reaches the ground. The images indicate that in both cases, the flame completely covers the ceiling within 0.3 s after ignition. Within the initial 0.1 s, the temperature of the majority of the combustion products rises to a range of 1300–1500 K. Subsequently, due to the rapid cooling effect of

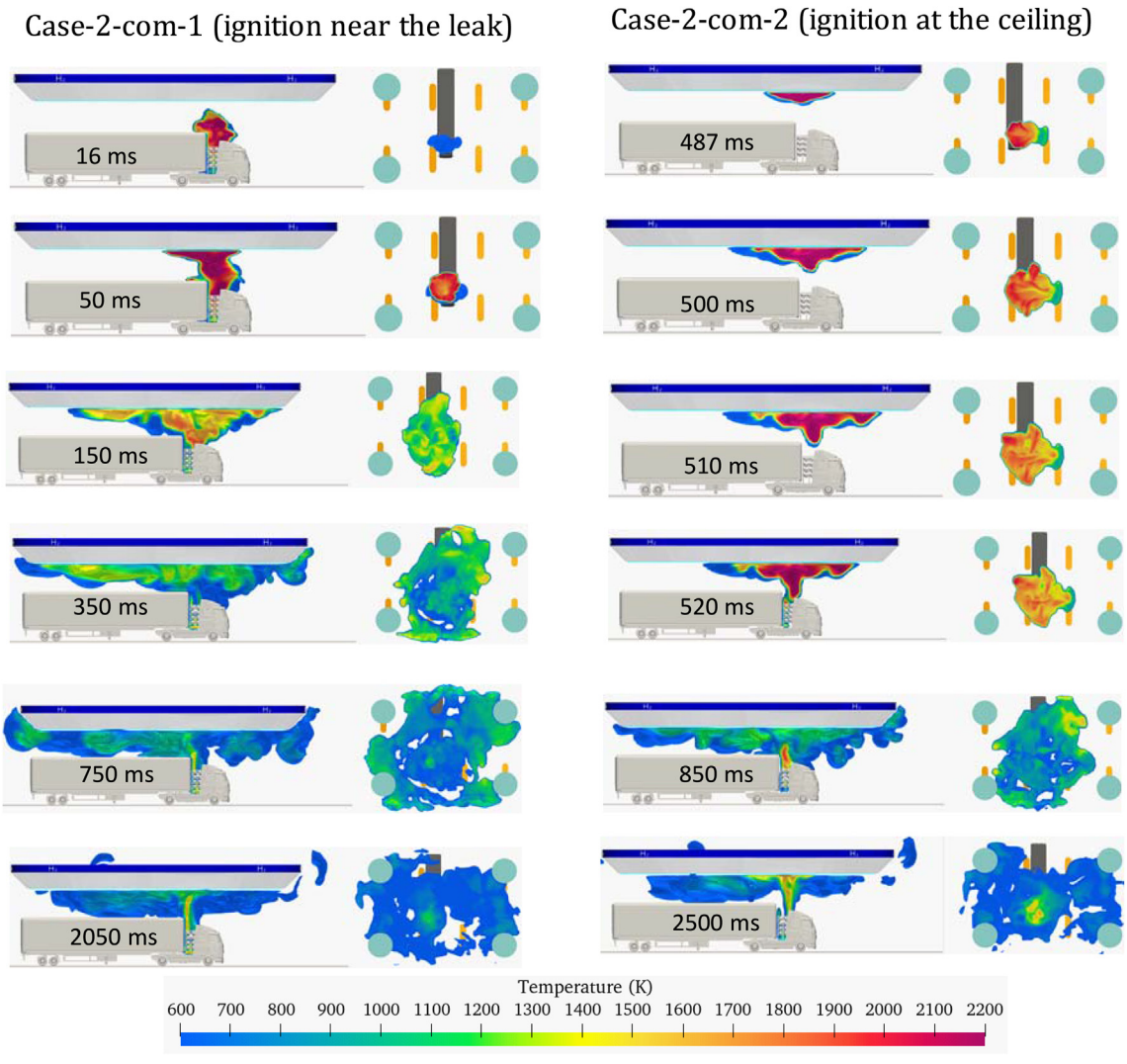

Fig. 8 – Temperature of hydrogen combustion products. (Vertical cut: Y = 4.9 m, horizontal cut: Z = 4.95 m).

the environment, the temperature decreases to 500–700 K within 2 s, irrespective of the ignition position.

3.5. *Harm analysis*

- **Fire hazards**

Hydrogen fire hazards cause exposure of people, components, or structures to flames, high air temperatures, or heat fluxes. The size, intensity, and duration of hydrogen fires depend on the type of hydrogen release and accident scenario. In the context of hydrogen fires, direct flame contact, including the hot gases released by flames, can be conservatively assumed to be lethal [28]. Data on burn mortality can be utilized to calculate the probability of a fatality. Delayed ignition accidents, like flash fires or burnable cloud explosions, can also cause direct flame contact. In such accidents, individuals located within the flammability limit boundary, defined as a hydrogen volume fraction of 4–75%, at the time of ignition, can be assumed to be fatal because of very high convective heat flux of 50–500 kW/m^2 even for slow subsonic flames [34]. Fig. 5 depicts the burnable cloud, which reveals that the lethal zone exists beneath the ceiling but above the truck container. The temperature profiles in Fig. 8 confirm that lethal flames typically do not directly contact individuals, except for those within 2–3 m of the hydrogen release. It should be noted that this assessment is highly conservative for flash fires and applies more accurately to jet fires, which could prolong the flame contact time.

The harm criteria used in our current scenario include [28,35], 1) thermal radiant intensity of 12.5–15 and 25 kW/m^2 for a duration of 10 s, leading to first-degree and significant injuries, respectively; and 2) a thermal dose threshold of 80–130 (kW/m^2)$^{4/3}$s, resulting in first-degree burns. These parameters are crucial in assessing potential harm caused by thermal radiation and establishing safety protocols for protecting individuals in high-risk environments. Fig. 9 illustrates the radiant heat flux on the ground and below the ceiling in both combustion cases. The maximum radiant heat flux of 250 kW/m^2 is observed above the hydrogen release location, which then drops rapidly to 50 kW/m^2 within 0.1 s and eventually reaches approximately 2 kW/m^2 in 2 s. It can be inferred that individuals standing on the ground in areas where the radiant heat flux is lower than that beneath the ceiling are not at risk of heavy harm. The impact of thermal heat fluxes from hydrogen fires on structures and equipment requires exposure times that are very long (>30 min) [28]. Therefore, this impact is generally not significant during the duration of a hydrogen fire, regardless of the combustion conditions.

- **Overpressure hazards**

Overpressures resulting from hydrogen deflagrations varies significantly depending on the specific scenario. In the event of a large release of hydrogen that mixes with air, a large flammable cloud may form before ignition takes place. The overpressure resulting from the cloud explosion is primarily determined by the speed of flame propagation. A deflagration event, characterized by a subsonic flame front, can produce overpressure effects on humans and structures. Conversely, a detonation event, which involves a supersonic flame front, can produce more significant overpressures. The presence of turbulence in the hydrogen release, unburned gases, and the presence of objects may potentially cause a transition from a deflagration to a detonation event. It is worth noting that hydrogen releases occurring in semi-confined zones, such as refueling stations with a roof, carry a higher risk of explosion than those that occur in completely open zones.

The direct effect of a sudden significant increase of pressure may result in damage to pressure-sensitive organs, such as the lungs and eardrums, while indirect effects arise from the impact of flying fragments and debris generated by the hydrogen explosion, as well as the collapse of structures. Moreover, large-scale explosions can propel individuals a considerable distance, exposing them to potential injury from collisions with structures or other violent movements. The criteria table contains examples of the overpressure necessary to cause harm to both humans and structures [28]. Furthermore, it is desirable in hydrogen safety assessment to use models that provide the probability of damage or harm as a function of the peak overpressure and/or the associated impulse. Fig. 10 shows the percentage of human fatality and structure failure according to the transformations of Eisenberg models, respectively. The largest overpressure 70 kPa leads to 100% structure failure, but cannot cause human death due to lung hemorrhage. The 3D visualization of the probability of human fatality and structure failure is involved in the next step of code development.

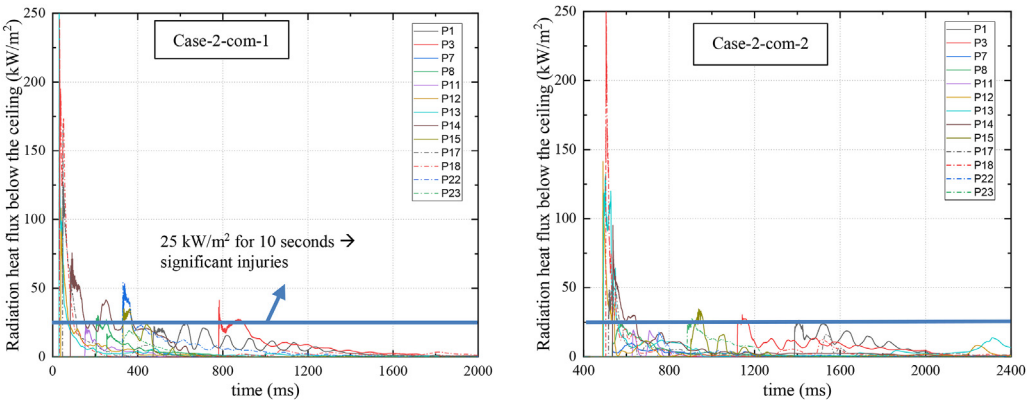

Fig. 9 – Radiant heat flux below the ceiling in Case-2.

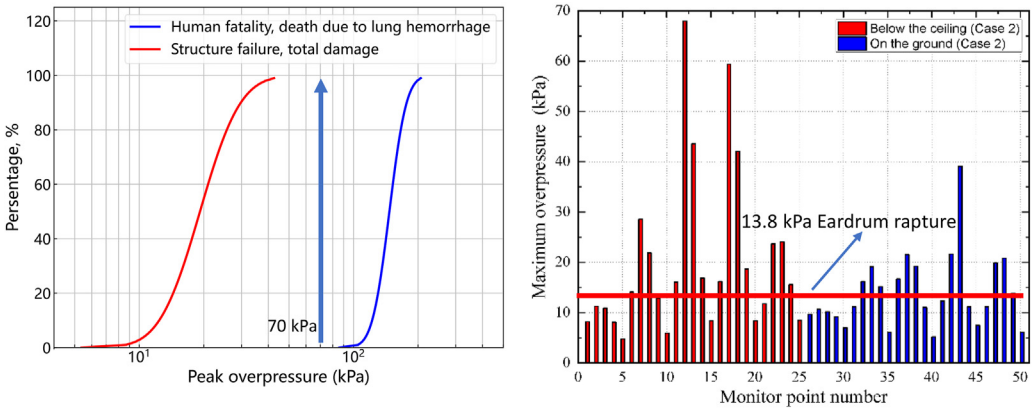

Percentage of human fatality and structure failure

Maximum overpressure in Case 2-Com-1

Fig. 10 – Overpressure hazards.

Fig. 10 reveals that the majority of maximum overpressure values fall within the range of 20 kPa, with the highest value being approximately 70 kPa. Consequently, there exists a high probability of eardrum rupture, although lung hemorrhage is not a concern. Fig. 10 corroborates that, for overpressure levels below 70 kPa, there is no possibility of human fatality, but the overpressure 70 kPa can lead to 100% structure failure. However, at some monitoring points, the maximum overpressure surpasses the threshold 48.3 kPa for internal injuries caused by the blast, but remains below the threshold for immediate blast fatalities 482.6 kPa. Nonetheless, for the current maximum overpressure of ~70 kPa, indirect effects are responsible for 100% human fatality from missile wounds. Further, Fig. 10 also highlights that the percentage of structure failure is also exceedingly high. Thus, it can be inferred that indirect effects stemming from overpressure events pose the primary threat to human safety. The underlying reason for this observation is that the threshold for fatal lung injury caused by overpressure is notably higher than the magnitude required for propelling individuals into obstacles or generating penetrating missiles. In addition, individuals who are situated within a structure during an overpressure event are at a greater risk of experiencing lethal injuries from the collapse of the facility rather than through direct lung damage.

Not only the overpressure threshold is the criterion for damage to structures but also the impulse or duration of pressure load, according to the diagrams of overpressure impulse in Ref. [35], the pressure impulse of 150–170 Pa*s corresponding to case 2-com-1 is probably not destructive to normal buildings on the ground level, but glass panels are likely to fail. Therefore, the flying fragments could injure people. Lung damage would not occur from your computed pressure peaks. But eardrum rupture could not be excluded, and temporary hearing loss is almost certain.

- **Hazard distance**

Employing engineering approaches can define hazard distances and predict overpressure effects during accidents. The overpressure caused by the blast wave decreases as the distance from the center of the burnable cloud increases. To determine the hazard distances, a conservative correlation has been developed by Ref. [32] without taking into account the hydrogen inventory and pressure impulse, which however can be utilized to approximate the blast wave overpressure that corresponds to the selected harm or damage criterion for specified parameters of hydrogen storage and release.

$$R = d\left(\frac{P_s}{P_0}\right)^{0.25}\left(5000\frac{P_0}{\Delta P_{criteria}}\right)^{1/1.9}, \tag{8}$$

where R is the hazard distance, d is the orifice diameter, P_s is the hydrogen storage pressure, P_0 is the ambient pressure, and $\Delta P_{criteria}$ is the overpressure of the harm criteria.

This approach aims to estimate the hazard distances from a source of overpressure hazard to prevent harmful effects on human beings. A "no-harm" overpressure threshold of 1.35 kPa is considered according to the harm criteria proposed in Ref. [36]. To assess the hazard distances caused by blast wave overpressure from a delayed ignition, the harm criteria for humans are applied. Specifically, the "slight injury" and "serious injury" thresholds are taken as 13.8 kPa and 48.3 kPa,

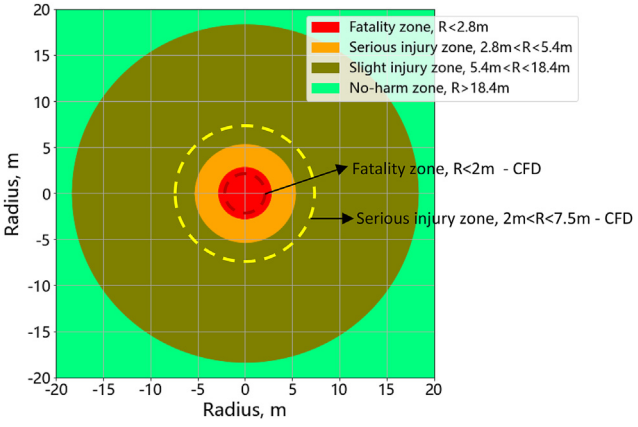

Fig. 11 – Hazard distances evaluated by correlation and CFD.

respectively. Overpressure beyond 48.3 kPa indicates "Fatality" due to indirect effects from missile wounds. The "slight injury" represents the direct effect of the threshold for eardrum rupture and the indirect effect of potential fatality from being projected against obstacles. The "serious injury" denotes the direct effect of 50% probability of eardrum rupture and the threshold of internal injuries caused by the blast, as well as the indirect effect of a 100% probability of fatality from missile wounds.

In the current case study, the hydrogen storage pressure is 35 MPa, the orifice diameter is 5 mm in Case 2, and the ambient pressure is 1 bar. Based on the above criteria, the distances of "no-harm," "slight injury," and "serious injury" are 18.4, 5.4, and 2.8 m, respectively, as illustrated in Fig. 11.

Fig. 12 depicts the overpressure contours between 13.8 and 48.3 kPa when Z < 2 m. The horizontal cut at 24 ms indicates a distance of 7.5 m, where humans were slightly injured. Furthermore, the threshold of 48.3 kPa at 11 ms is at a distance of approximately 2 m. In comparison to the results obtained from empirical correlations, as presented in Fig. 11, the CFD predictions suggest that the human fatality zone is smaller, while the serious injury zone is larger.

4. Conclusions

In this study, the deterministic risk assessment approach is used for risk assessment in of hydrogen leakage in a real-scale

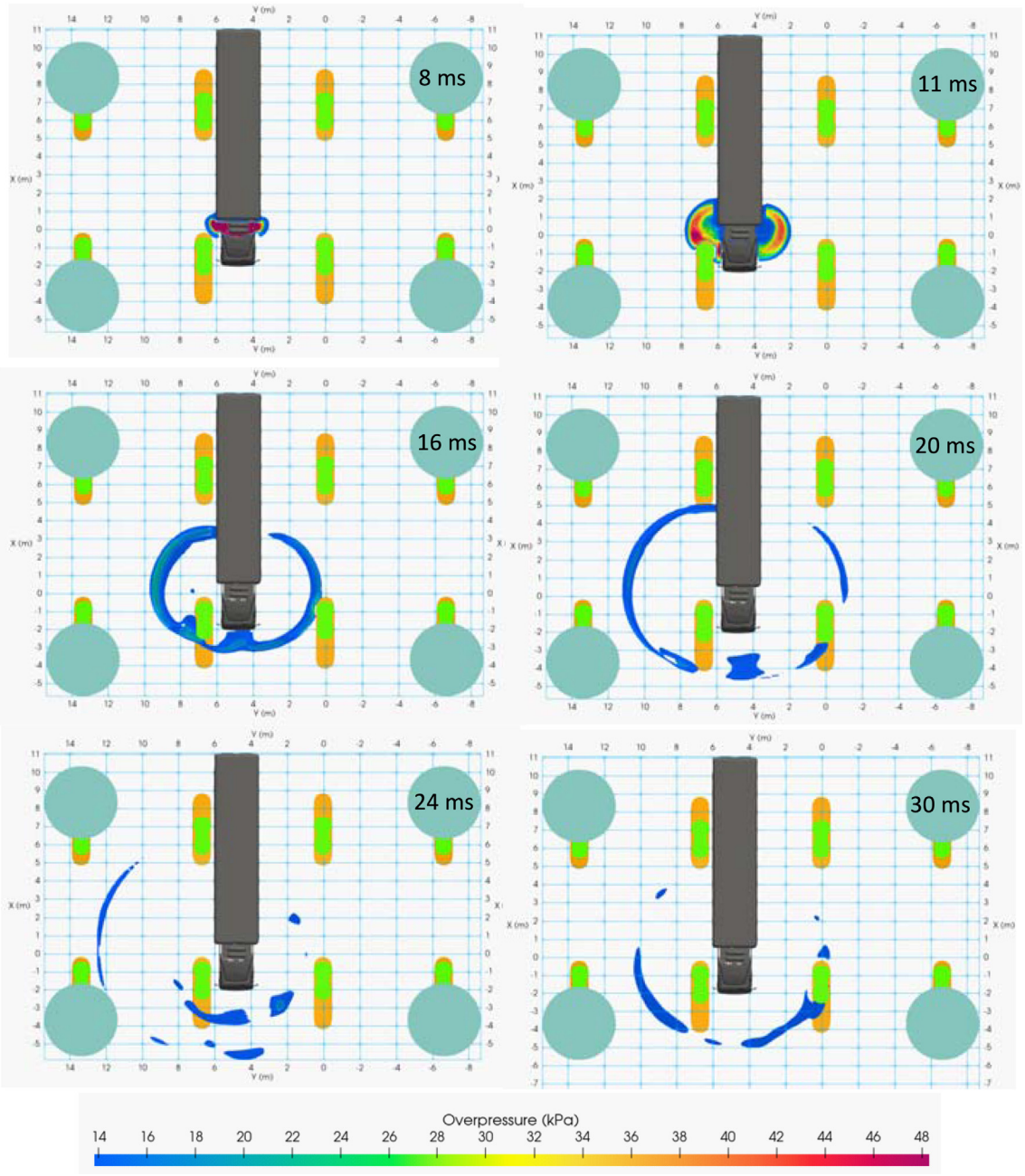

Fig. 12 – Overpressure contours 13.8–48.3 kPa (Z < 2 m, Case-2-com-1, ignition near the leak).

hydrogen refueling station. This approach requires the description of scenarios, 3D CFD simulations, consequence assessment, etc. The main steps involved in the implementation of DRA consist of importing a 3D geometry model, identifying the worst-scenarios, generating the hydrogen release sources, initializing hazardous materials and boundary conditions, simulating the hydrogen dispersion, simulating jet/flash fire, simulating explosion scenarios, visualizing thermal and overpressure load contours, estimating the harm on human and structure, and evaluating the risk. DRA complements the traditional approach QRA considerably by providing interactive 3D information for risk assessment and management within organizations. However, a complete implementation requires a dedicated user responsible for conducting CFD simulations and risk assessments, which could cause human errors and biases in the risk assessments.

GASFLOW-MPI serves as a CFD tool for investigating the impinging jet, dispersion, and combustion of hydrogen in a real complex geometry, providing detailed insights compared to predictions from fast-running models. CFD simulations of the phenomena in wide ranges (from hydrogen dispersion to hydrogen deflagration and explosion) reveal the importance and strength of the all-speed CFD in hydrogen safety assessment. GASFLOW-MPI together with the engineering hydrogen release and consequence evaluation models are adopted to verify the DRA approach for identifying the potential hazards posed by a hydrogen leak from a truck under a large roof of a real hydrogen station. Results show that:

The roof configuration may lead to a burnable cloud of hydrogen accumulating below the ceiling. In the current case, a maximum mass of 2 kg, volume of 130 m^3, and 90% of the hydrogen stores under the ceiling half-meter. However, this burnable cloud rapidly diminishes in less than a minute. When the roof is absent, the burnable hydrogen mass exhibits a smaller peak and a quicker decay. In the event of a delayed ignition, the largest overpressure recorded on the ceiling and ground amounted to 65 kPa and 38 kPa, respectively. While the thermal radiation exposure to individuals on the ground was deemed insignificant, the overpressure results in structural failure with a high probability, which could indirectly lead to human fatalities. This case study provides valuable insights into the potential risks associated with hydrogen leaks, particularly in semi-confined hydrogen refueling stations with large roofs. In light of these risks, it is recommended that standards should be developed to limit the maximum roof coverage of installations, which could promote the development of a safer hydrogen energy infrastructure.

The planned tasks for the future include studying the effect of roof inclination and configuration, implementing H_2 risk mitigation measures, conducting PSA analysis to identify accident scenarios, and developing fast-evaluating models, etc.

Author contributions

Conceptualization and methodology, J.X. and F.W.; software, J.X.; formal analysis, J.X. and F.W.; writing—original draft preparation, J.X. and F.W.; writing—review and editing, M.K., W.B., B.H., S.R., S.Z., T.J., K.S. and L.Z.; All authors have read and agreed to the published version of the manuscript.

Declaration of competing interest

The authors declare that they have no known competing financial interests or personal relationships that could have appeared to influence the work reported in this paper.

Acknowledgements

This work is supported by Innovations pool project 2021-2023 from Helmholtz-Forschungsbereich Energie – Programm MTET Zukunftsthema "Solarer Wasserstoff – hochrein und komprimiert", Grant: 38.02.02, 38.04.03, 38.05.01.

REFERENCES

[1] The International Energy Agency (IEA). The Hydrogen Technology Collaboration Programme (Hydrogen TCP), Available [01.05.2023]: www.ieahydrogen.org.
[2] Molkov V. Fundamentals of hydrogen safety engineering. Bookboon. com; 2012. p. 978–87. ISBN.
[3] Breitung W, Royl P. Procedure and tools for deterministic analysis and control of hydrogen behavior in severe accidents. Nucl Eng Des 2000;202(2–3):249–68.
[4] Pagliaro M, Iulianelli A. Hydrogen refueling stations: safety and sustainability. General Chemistry 2020;6(1):190029.
[5] Xiao J, Breitung W, Kuznetsov M, Zhang H, Travis JR, Redlinger R, Jordan T. GASFLOW-MPI: a new 3-D parallel all-speed CFD code for turbulent dispersion and combustion simulations Part II: first analysis of the hydrogen explosion in Fukushima Daiichi Unit 1. Int J Hydrogen Energy 2017;42(12):8369–81.
[6] Aven T. Risk, surprises and black swans: fundamental ideas and concepts in risk assessment and risk management. Routledge; 2014.
[7] Groth KM, Hecht ES. HyRAM: a methodology and toolkit for quantitative risk assessment of hydrogen systems. Int J Hydrogen Energy 2017;42(11):7485–93.
[8] Skjold T, Siccama D, Hisken H, Brambilla A, Middha P, Groth KM, LaFleur AC. 3D risk management for hydrogen installations. Int J Hydrogen Energy 2017;42(11):7721–30.
[9] Middha P, Hansen OR. Using computational fluid dynamics as a tool for hydrogen safety studies. J Loss Prev Process Ind 2009;22(3):295–302.
[10] Xiao J, Breitung W, Kuznetsov M, Zhang H, Travis JR, Redlinger R, Jordan T. GASFLOW-MPI: a new 3-D parallel all-speed CFD code for turbulent dispersion and combustion simulations: Part I: models, verification and validation. Int J Hydrogen Energy 2017;42(12):8346–68.
[11] Choi J, Hur N, Kang S, Lee ED, Lee KB. A CFD simulation of hydrogen dispersion for the hydrogen leakage from a fuel

cell vehicle in an underground parking garage. Int J Hydrogen Energy 2013;38(19):8084–91.
[12] Usman A, Rafiq M, Saeed M, Nauman A, Almqvist A, Liwicki M. Machine learning computational fluid dynamics. In: 2021 Swedish artificial intelligence society workshop (SAIS). IEEE; 2021, June. p. 1–4.
[13] Choi O, Lee MC. Investigation into the combustion instability of synthetic natural gases using high speed flame images and their proper orthogonal decomposition. Int J Hydrogen Energy 2016;41(45):20731–43.
[14] Pramuanjaroenkij A, Kakaç S. The fuel cell electric vehicles: the highlight review. Int J Hydrogen Energy 2023;48(25):9401–25.
[15] Mukai S, Suzuki J, Mitsuishi H, Watanabe S. CFD simulation of diffusion of hydrogen leakage caused by fuel cell vehicle accident in tunnel, underground parking lot and multistory parking garage. JARI Research Journal 2005;27(9):505.
[16] Hirt CW, Amsden AA, Cook JL. An arbitrary Lagrangian-Eulerian computing method for all flow speeds. J Comput Phys 1974;14(3):227–53.
[17] Harlow FH, Amsden AA. A numerical fluid dynamics calculation method for all flow speeds. J Comput Phys 1971;8(2):197–213.
[18] Zhang H, Li Y, Xiao J, Jordan T. Detached Eddy Simulation of hydrogen turbulent dispersion in nuclear containment compartment using GASFLOW-MPI. Int J Hydrogen Energy 2018;43(29):13659–75.
[19] Zhang H, Li Y, Xiao J, Jordan T. Large eddy simulations of the all-speed turbulent jet flow using 3-D CFD code GASFLOW-MPI. Nucl Eng Des 2018;328:134–44.
[20] Wang F, Xiao J, Jordan T. GASFLOW-MPI analysis on deflagration in full-scale hydrogen refueling station experiments: H2-air premixed cloud and high-pressure H2 jet. Int J Hydrogen Energy 2022;47(32):14725–39.
[21] Xiao J, Travis JR, Kuznetsov M. Numerical investigations of heat losses to confinement structures from hydrogen-air turbulent flames in ENACCEF facility. Int J Hydrogen Energy 2015;40(38):13106–20.
[22] Xiao J, Kuznetsov M, Travis JR. Experimental and numerical investigations of hydrogen jet fire in a vented compartment. Int J Hydrogen Energy 2018;43(21):10167–84.
[23] Xiao J, Breitung W, Kuznetsov M, Zhang H. Numerical investigations of turbulent slow deflagration of premixed H2-air-H2O mixture in Thai test HD-22 using CFD code GASFLOWMPI. In: 17th international topical meeting on nuclear reactor thermal hydraulics; 2017, September. NURETH-17).
[24] Xiao J, Breitung W, Kuznetsov M, Travis J, Redlinger R. Development and validation of the parallel all-speed CFD code GASFLOW-MPI for detonation of premixed H2-air mixture in a hemispherical balloon. International Conference on Nuclear Engineering 2017, July;57861:V008T09A003 [American Society of Mechanical Engineers].
[25] Hecht E, Ehrhart B. Hydrogen plus other alternative fuels risk assessment models (HyRAM+) version 4.0 technical reference manual (No. SAND2021-14813). Albuquerque, NM (United States): Sandia National Lab.(SNL-NM); 2021.
[26] Travis JR, Koch DP, Breitung W. A homogeneous non-equilibrium two-phase critical flow model. Int J Hydrogen Energy 2012;37(22):17373–9.
[27] Hosseini M, Dincer I, Naterer GF, Rosen MA. Thermodynamic analysis of filling compressed gaseous hydrogen storage tanks. Int J Hydrogen Energy 2012;37(6):5063–71.
[28] LaChance J, Tchouvelev A, Engebo A. Development of uniform harm criteria for use in quantitative risk analysis of the hydrogen infrastructure. Int J Hydrogen Energy 2011;36(3):2381–8.
[29] Eisenberg NA, Lynch CJ, Breeding RJ. Vulnerability model. A simulation system for assessing damage resulting from marine spills. Enviro control inc rockville md; 1975.
[30] http://www.beijing.gov.cn/ywdt/zwzt/xyesd/zxdt/202210/t20221019_2838908.html.
[31] Li Y, Xiao J, Zhang H, Breitung W, Travis J, Kuznetsov M, Jordan T. Numerical analysis of hydrogen release, dispersion and combustion in a tunnel with fuel cell vehicles using all-speed CFD code GASFLOW-MPI. Int J Hydrogen Energy 2021;46(23):12474–86.
[32] Cirrone D, Makarov D, Friedrich A, Grune J, Takeno K, Molkov V. Blast wave generated by delayed ignition of under-expanded hydrogen free jet at ambient and cryogenic temperatures. Hydro 2022;3(4):433–49.
[33] Wang F, Zou Z, Deng J, Qin H, Zhang M. Investigations of hydrogen hazard mitigation by deliberate ignition in small modular reactor during severe accident using GASFLOW-MPI. Ann Nucl Energy 2022;179:109392.
[34] Kuznetsov M, Matsukov I, Dorofeev S. Heat loss rates from hydrogen-air turbulent flames in tubes. Combust Sci Technol 2002;174(10):75–92.
[35] Yanez J, Kuznetsov M, Souto-Iglesias A. An analysis of the hydrogen explosion in the Fukushima-Daiichi accident. Int J Hydrogen Energy 2015;40(25):8261–80.
[36] Baker WE, Cox PA, Kulesz JJ, Strehlow RA, Westine PS. Explosion hazards and evaluation. Elsevier; 2012.